



Article

The Suppression Effect of Water Mist Released at Different Stages on Lithium-Ion Battery Flame Temperature, Heat Release, and Heat Radiation

Bin Miao ^{1,2,3} , Jiangfeng Lv ¹, Qingbiao Wang ^{1,2,4,*}, Guanzhang Zhu ⁵ , Changfang Guo ⁶, Guodong An ⁷ and Jianchun Ou ⁸

¹ College of Resources, Shandong University of Science and Technology, Tai'an 271019, China; miaobin@sust.edu.cn (B.M.)

² National Engineering Laboratory for Coalmine Backfilling Mining, Tai'an 271019, China

³ Zaozhuang Mining Group Co., Ltd, Zaozhuang 277000, China

⁴ School of Civil Engineering, Shandong Jianzhu University, Jinan 250101, China

⁵ Beijing Tianma Intelligent Control Technology Co., Ltd., Beijing 101399, China

⁶ Artificial Intelligence Research Institute, China University of Mining and Technology, Xuzhou 221116, China

⁷ Jining Haida Xingzhi School, Jining 272100, China

⁸ State Key Laboratory for Fine Exploration and Intelligent Development of Coal Resources, China University of Mining and Technology, Xuzhou 221116, China

* Correspondence: skd990748@sust.edu.cn

Abstract: Thermal runaway (TR) is a serious thermal disaster that occurs in lithium-ion batteries (LIBs) under extreme conditions and has long been an obstacle to their further development. Water mist (WM) is considered to have excellent cooling capacity and is widely used in the field of fire protection. When used in TR suppression, WM also exhibits strong fire-extinguishing and anti-re-ignition abilities. Therefore, it has received widespread attention and research interest among scholars. However, most studies have focused on the cooling rate and suppression effect of TR propagation, and few have mentioned the effect of WM on flame heat transfer, which is a significant index in TR propagation suppression. This study has explored the suppression effect of WM released at different TR stages and has analyzed flame temperature, heat release, and heat radiation under WM conditions. Results show that the flame extinguishing duration for WM under different TR stages was different. WM could directly put out the flame within several seconds of being released when SV opened, 3 min after SV opening and when TR ended, and 3 min for WM when TR was triggered. Moreover, the heat radiation of the flame in relation to the battery Q_E could be calculated, and the case of WM released 3 min after SV opening exhibited the greatest proportion of heat radiation cooling η (with a value of 88.4%), which was same for the specific cooling capacity of WM Q_m with a value of 1.7×10^{-3} kJ/kg. This is expected to provide a novel focus for TR suppression in LIBs.

Keywords: lithium-ion battery; thermal runaway; water mist suppression; flame heat release; flame heat radiation



Citation: Miao, B.; Lv, J.; Wang, Q.; Zhu, G.; Guo, C.; An, G.; Ou, J. The Suppression Effect of Water Mist Released at Different Stages on Lithium-Ion Battery Flame Temperature, Heat Release, and Heat Radiation. *Batteries* **2024**, *10*, 232. <https://doi.org/10.3390/batteries10070232>

Academic Editor: Mingyi Chen

Received: 6 May 2024

Revised: 4 June 2024

Accepted: 7 June 2024

Published: 28 June 2024



Copyright: © 2024 by the authors. Licensee MDPI, Basel, Switzerland. This article is an open access article distributed under the terms and conditions of the Creative Commons Attribution (CC BY) license (<https://creativecommons.org/licenses/by/4.0/>).

1. Introduction

Lithium-ion batteries (LIBs) are widely used in electronic devices, electric vehicles, aerospace, and electrochemical energy storage, owing to their advantages of high energy density, a high-voltage platform, high charging and discharging efficiency, environment friendliness, a long lifespan, and wide applicability [1–5]. In practical appliance scenarios consisting of high energy densities, prismatic batteries stand out among other batteries, such as 18,650 batteries and pouch batteries, due to their large capacity [6]. However, a large capacity also constitutes a high thermal hazard in the process of thermal runaway (TR) [7]. The TR process is a severe exothermic disaster in LIBs, with the phenomena of combustible gases and jet flames [8]. Under extreme conditions, such as external heating, overcharging,

penetration, and friction, the TR process may be triggered but not terminated [9,10]. In the process of TR, a series of pyrolysis side reactions are triggered continuously among the active materials inside the battery, exhibiting a high heat release rate, a high battery surface temperature, violent combustible gas release, and a serious risk of combustion and explosion [11–13]. Moreover, the process of TR in a single LIB will generally propagate to the adjacent batteries, ultimately resulting in a large-scale TR process in the LIB module, which will cause casualties and property damage [14,15].

The TR process in the LIB is both related to internal and external factors. The internal factors of commonly used LIBs mainly include the cathode material, the state of charge (SOC), the state of health (SOH), and the rated capacity [16,17]. The commonly used battery cathode materials are nickel cobalt manganese ternary lithium (NCM), nickel cobalt aluminum ternary lithium (NCA), and lithium iron phosphate (LFP). NCM and NCA batteries have a higher energy density but poorer thermal stability than LFP batteries, and they exhibit a fiercer TR process for a greater heat release rate and gas generation rate [18,19]. With the decline in battery SOC, the TR process becomes weaker and even disappears. In batteries with a high SOC, there are more lithium ions embedded in the anode material, which directly accelerates the side reactions of TR and reduces the TR triggering temperature [20]. The SOH does not directly affect the TR intensity, but it is more likely for lithium deposition and lithium dendrite growth to appear in the batteries with low SOH under extreme abuse conditions, causing a lower TR triggering temperature and charging security [21]. A battery with a higher-rated capacity will generate more heat and gases in its TR process due to a larger amount of active materials inside the battery [4]. The external factors mainly include the TR triggering method, the external oxygen content, and the ambient pressure. There are various thermal hazards of LIBs under external heating, overcharging, and penetration conditions. Most TR hazards occur under overcharging conditions, both in the single battery and the battery module [22,23]. When the oxygen content is low, the TR reactions inside the battery will be weakened, resulting in a lower surface temperature, mass loss, and heat release rate [24]. Additionally, under low or high ambient pressure levels, the TR hazard will be impaired, but the TR process is more likely to be triggered in low-pressure ambient environments [25].

In order to suppress the TR process and decrease the likelihood of a TR hazard, many scholars have tested different fire-extinguishing agents and suppression strategies [18,26,27]. The typical fire-extinguishing agents for LIBs are gaseous fire-extinguishing agents, dry powders, water-based fire-extinguishing agents, and aerosol fire-extinguishing agents. Zhang [28] has investigated the TR suppression effect of CO₂, HFC-227ea, and C₆F₁₂O and found that C₆F₁₂O could immediately extinguish the flame, CO₂ needed a longer duration for flame extinguishing, and HFC-227ea could not suppress the flame. Sun [29] has investigated the suppression effect of HFC-227ea and C₆F₁₂O for TR propagation purposes and found that HFC-227ea could hardly suppress its propagation and C₆F₁₂O could prolong the propagation time. Zhao [30] has investigated the TR suppression effect of ABC and BC ultrafine dry powders and found that they could not suppress TR propagation due to their poor cooling capacity. Davion [31] has tested aerosols for TR suppression purposes and found that they could immediately extinguish the flame, but a re-ignition phenomenon occurred. Tang [32] found that F500 had a good suppression effect for LIB TR. Liu [33] has investigated the water mist (WM) cooling strategy for TR propagation purposes and found that WM exhibited an excellent cooling capacity and could easily prevent TR propagation in the LIB module. Zhang [34] combined N₂, C₆F₁₂O, and WM in TR suppression and found that N₂-twin-C₆F₁₂O mist could successfully inhibit the re-ignition of the battery flame and that the N₂-twin-H₂O mist synergistic technology could increase the cooling rate by over 20%. Li [35] added sodium dodecyl benzene sulfonate, sodium chloride and soy protein in WM and found with these additives, WM exhibited a greater cooling capacity and could cool down the LIB flame and surface temperature in a low duration. Zhang [36] has investigated the suppression effect of WM intermittent spray strategy for TR propagation and found this strategy could combine the advantages of

low water consumption and high cooling capacity. Mei [37] has compared the suppression effect of three TR retardants based on parameters including flame height, and these novel retardants all expressed a greater TR suppression effect compared to paraffin.

Among various strategies for TR suppression, WM demonstrates outstanding cooling capacity and can effectively prevent battery flame re-ignition. However, existing studies predominantly focus on WM's cooling rate and its impact on TR propagation, largely overlooking its influence on flame heat transfer. When battery flames occur, the heat transferred from the flame to adjacent batteries similarly influences TR propagation dynamics. Therefore, investigating WM's cooling effects on LIB flames is crucial. This study has explored the suppression effect of WM released at different TR stages and has analyzed flame temperature, heat release, and heat radiation under WM conditions, aiming to introduce a new perspective on TR suppression in LIBs.

2. Experimental Settings

2.1. Battery Sample

The experimental batteries used were 100 Ah prismatic LFP batteries manufactured by Lishen (Qingdao). They consisted of a lithium iron phosphate (LiFePO_4) cathode, layered graphite (C) anode, aluminum (Al) positive current collector, copper (Cu) negative current collector, and an electrolyte mixture of ethylene carbonate (EC), propylene carbonate (PC), and dimethyl carbonate (DMC). The separator was polyethylene microporous membrane (PE), and the battery shell was aluminum (Al). Each battery was equipped with a safety valve (SV) to release gases during extreme conditions. The dimensions of each battery were $220 \text{ mm} \times 140 \text{ mm} \times 35 \text{ mm}$, with a mass of $2160 \pm 2 \text{ g}$. Prior to experiments, all battery samples had their plastic covers removed. During charging and discharging, the maximum cut-off voltage was set at 3.6 V and the minimum at 2.5 V. Each battery underwent 3 cycles of charging/discharging, followed by a full charge to 100% State of Charge (SOC) using a Neware cyler and a 12-h rest period after each cycle. Each cycle included phases of constant current charging, constant voltage charging, and constant current discharge.

2.2. Experimental Setup

The schematic diagram of the experimental setup is shown in Figure 1. The experimental platform was constructed according to the standard of ISO 9705 [38]. The experiments of LIB TR and WM suppression were conducted in the combustion chamber where the observation window and WM nozzle were. The exhausting fume collecting hood was equipped at the top of the combustion chamber, and a fan was equipped at the end of the smoke exhaust duct with an exhaust volume of $0.13 \text{ m}^3/\text{s}$. A supply pipe for WM was installed in the combustion chamber and a WM pump was connected to the pipe ending. The WM-released pressure and mass flow were 6.5 MPa and 0.4 L/min, respectively.

The experimental module consisted of, a stainless steel module framework, two mica insulation plates, an LFP battery sample, and the heating plate. The dimension of the heating plate was the same as the battery sample, and the dimension of the mica insulation plate was slightly larger than the battery sample. The power of the heating plate was 500 W, and heating was stopped when TR was triggered or WM was released. One type K armored thermocouple was installed at the center of the battery surface and five were installed 10, 30, 50, 70, and 90 cm above the SV in order to monitor the temperature of the battery surface and flame. The measurement span, accuracy, and recording frequency of each type K armored thermocouple were $-100\text{--}1200 \text{ }^\circ\text{C}$, $\pm 1.5\text{--}5 \text{ }^\circ\text{C}$, and 1 Hz, respectively. A disposable igniter was set in front of the experimental module. Once SV opened, the igniter was remotely activated, generating sparks to ignite the battery flame.

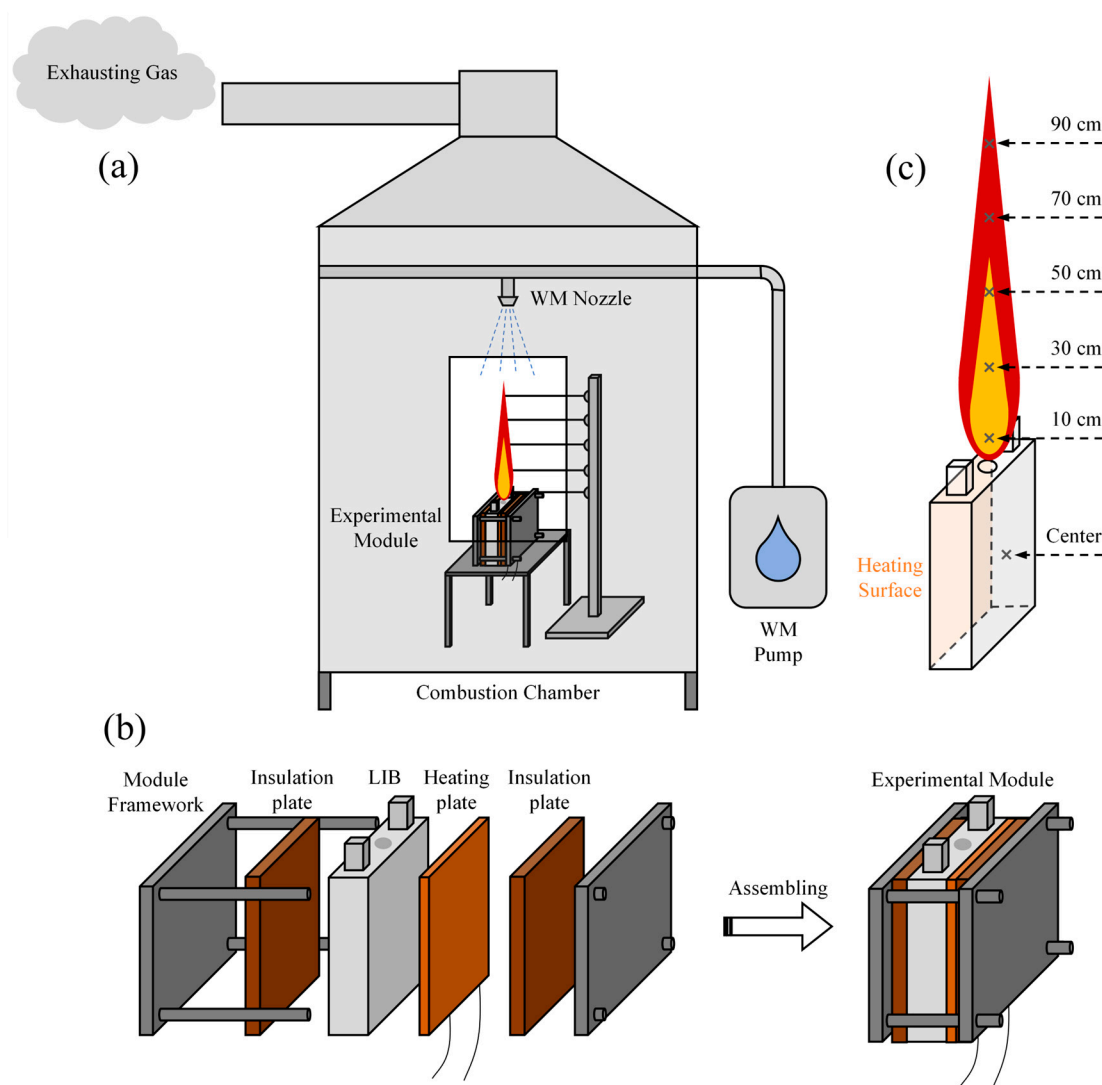


Figure 1. The schematic diagram of the experimental setup: (a) Experimental platform; (b) Experimental Module; (c) Thermocouple layout.

2.3. Case Setting

The experiment cases were set as Table 1 shown. In order to investigate the TR characteristic of the experimental battery sample, Case 1 was set to analyze the typical TR process and establish a reference for the extinguishing cases. Cases 2 to 5 were set to analyze the effect of WM on battery flame temperature and its heat release. In all the cases, the TR of the battery samples was triggered by external heating.

Table 1. Cases setting.

No.	WM Release Temperature	Case Description
Case 1	\	No WM extinguishing.
Case 2	108 °C	WM released at SV opening.
Case 3	116 °C	WM released 3 min after SV opening.
Case 4	140 °C	WM released at TR triggering.
Case 5	400 °C	WM released after TR ended.

3. Experimental Results and Analyses

3.1. Analysis of the Temperatures of Battery Surface and TR Flame

During thermal abuse conditions, the battery temperature generally rose due to heat transfer from an external heating plate, ultimately triggering the TR process accompanied by a vigorous jet flame. Figure 2 illustrates the curves of battery voltage, temperature, and temperature rise rate during the TR process.

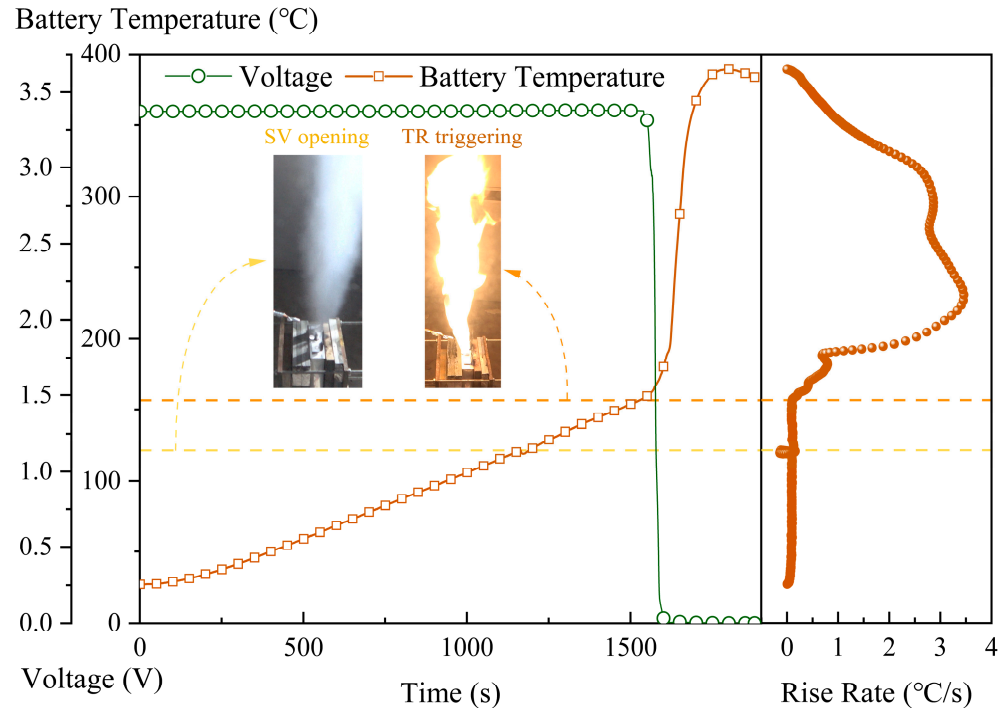
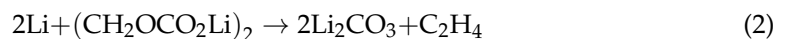
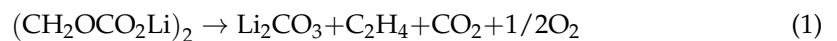
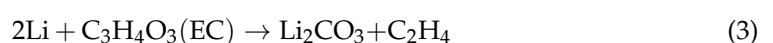


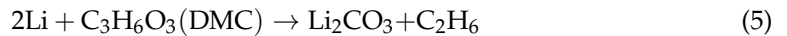
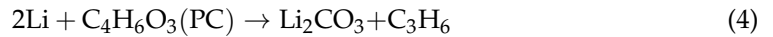
Figure 2. The curves of battery voltage, temperature, and its rise rate.

The battery temperature experienced a uniform rise, instantaneous descent, brief jumping ascent, and overall rapid rise, and they corresponded to the phenomena of external heating, SV opening, TR triggering, and TR peak. In the stage of external heating, with the internal temperature increase, the solid electrolyte interface (SEI) film was experiencing pyrolysis and slightly generated heat and combustible gases. When gases accumulated exceeded the threshold, SV was broken and a part of the heat was brought by the jet gas, resulting in the instantaneous descent of the temperature. The pyrolysis reactions of the SEI film are shown as follows [39]:

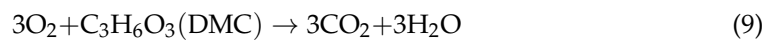
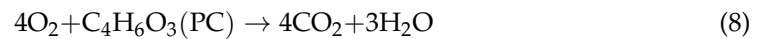
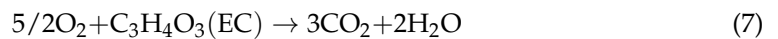
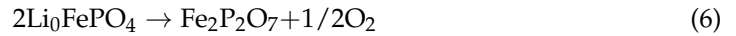


During the stage of TR triggering, the temperature rise rate initially increased and then decreased. Following the decomposition of the SEI film, lithium ions embedded in graphite came into direct contact with the organic electrolyte, releasing combustible gases and generating heat. Subsequently, lithium ions from the electrolyte deposited on graphite formed lithium dendrites that eventually bridged the cathode and anode, leading to internal short circuits and significant heat generation. This heat caused widespread melting of the separator, which absorbed some heat and contributed to a reduction in the temperature rise rate. Additionally, extensive internal short circuits occurring during this stage caused the battery voltage to plummet to 0 V. The pyrolysis reactions of the electrolyte are depicted as follows:





With increasing heat accumulation within the battery, the pyrolysis reaction of the cathode material initiates, marking the peak of the TR process. During this phase, extensive pyrolysis reactions ensue among the battery's internal active materials, generating significant heat and gases and causing the vaporization of the organic electrolyte. Consequently, the battery temperature rises rapidly. The pyrolysis reactions involving the cathode material LiFePO_4 and the electrolyte can be illustrated as follows:



The state of the battery flame was distinct from the TR process, and the curves of battery temperature and TR flame temperatures were 10, 30, 50, 70, and 90 cm above the SV, as shown in Figure 3.

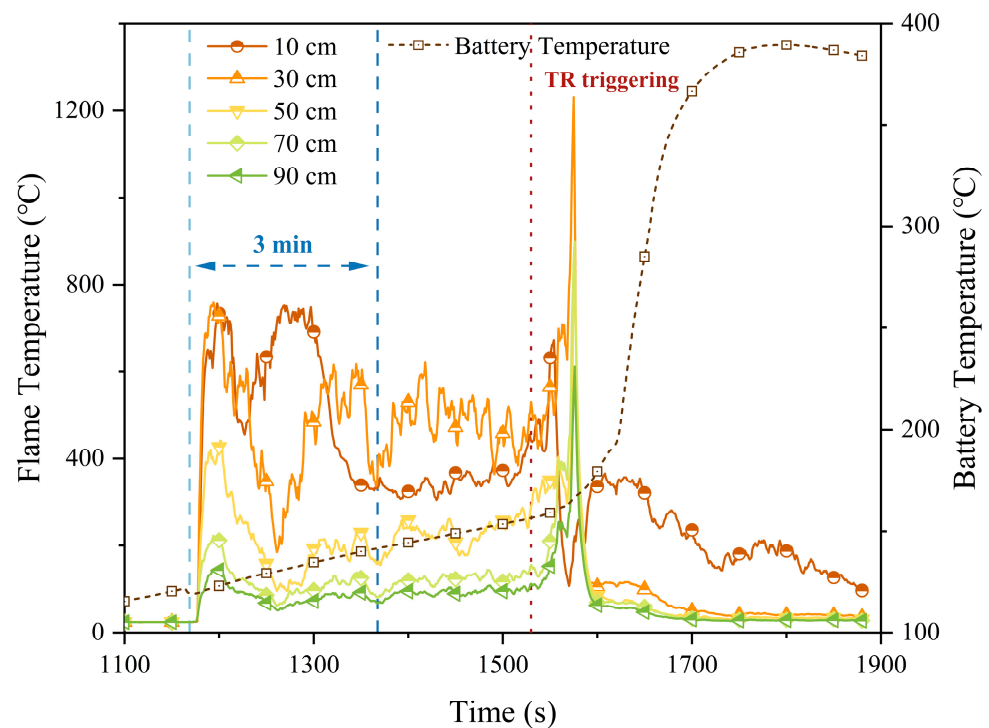


Figure 3. The curves of battery temperature and TR flame temperatures.

When the SV opened, combustible gases were expelled from the battery. Unlike the gases released after TR triggering, which predominantly contained organic electrolyte vapor, those released before TR were primarily inorganic gases like H_2 and CO , known for their higher calorific values, resulting in a higher flame temperature prior to TR triggering [40]. Approximately 3 min after SV opening, the battery flame temperature exhibited a regular fluctuation pattern, indicating stabilization thereafter, serving as a benchmark for WM release. During TR triggering, flame temperatures at various positions initially soared, then declined before stabilizing. At 30 cm, the maximum temperature exceeded 1200°C . It was noted that while temperatures at other positions rose, the flame temperature at 10 cm dropped significantly due to flame extinction caused by high-speed gas jets at the flame base.

3.2. Analysis of the Effect of WM on TR Flame

The flame characteristics, including velocity and temperature, varied with the progression of the TR process. Consequently, the impact of WM on the battery flame differed across different stages of TR: WM swiftly extinguished the flame within seconds of release upon SV opening, after 3 min of SV opening, and at TR termination. However, it took approximately 3 min for WM to extinguish the flame once TR was triggered. Figure 4 illustrates the temperature curves of the battery flame under the influence of WM.

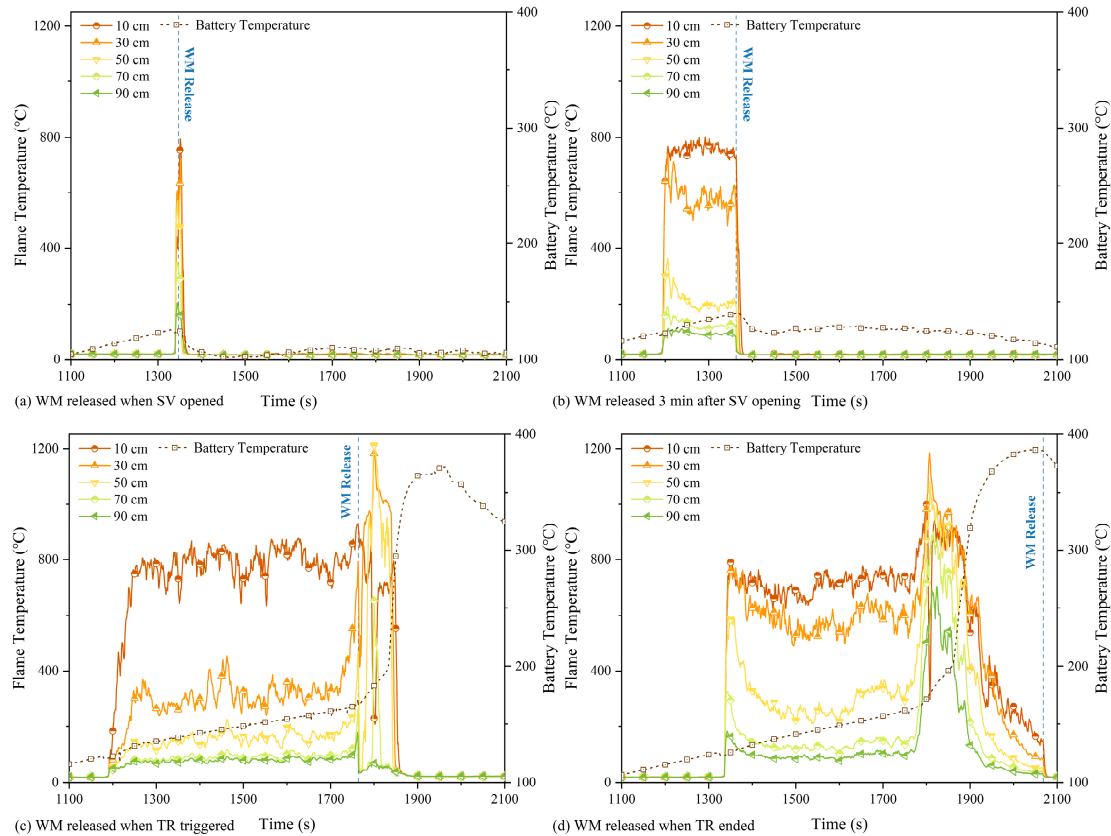


Figure 4. The curves of battery flame temperatures under the effect of WM: (a) WM released when SV opened; (b) WM released 3 min after SV opening; (c) WM released when TR triggered; (d) WM released when TR ended.

When WM was released before TR triggering, the battery flame could be extinguished immediately. During this phase, the gas generation rate was moderate, maintaining a stable flame that allowed WM droplets to effectively reach the flame's base and extinguish it. However, after TR triggering, the production of combustible gases accelerated significantly. Short-chain alkenes mixed with organic electrolyte vapor were expelled at high velocity, inducing a turbulent jet flame state. WM was less effective in suppressing this high-velocity flame and could only influence its upper portion, causing the flame to assume a conical shape. Before TR triggering, the flame temperature distribution showed lower temperatures at the top and higher temperatures at the bottom, with the region 10 cm above the SV exhibiting the highest temperature. However, due to the rapid jet gas velocity, the lower part of the flame experienced uneven oxygen mixing, leading to unstable combustion and resulting in higher temperatures observed at 30 and 50 cm above SV. Comparing the case of no WM release and release when TR triggered, the temperature at 30 and 50 cm were both greater in the case of WM released. This outcome occurred because WM suppressed the flame's upper region and concentrated the combustion into a smaller area, thereby elevating the core flame temperature. Upon TR cessation, the flame transitioned into an ember state, facilitating immediate extinguishment upon WM release.

3.3. Analysis of the Heat Cooling of TR Flame and Specific Cooling Capacity of WM

For disaster prevention and control, the heat release of battery flame is a key parameter. To calculate the heat release of battery flame Q , first, the heat flux density of battery flame q calculated by Equation (10) is needed [41].

$$q = h(T_{f,i} - T_a) \quad (10)$$

where $T_{f,i}$ and T_a are the flame temperature at i position and ambient temperature, respectively, and h is the convective heat transfer coefficient in the experimental environment which can be calculated by Equation (11). The Nusselt number Nu can be calculated by Equations (12)–(14) [42].

$$h = Nu \frac{\lambda}{d} \quad (11)$$

$$Nu = 0.27Re^{0.63}Pr^{0.36}(Pr_f/Pr_w)^{0.25} \quad (12)$$

$$Re = \frac{\rho v d}{\mu} \quad (13)$$

$$Pr = \frac{v}{\alpha} = \frac{v}{\lambda/\rho c} \quad (14)$$

where Re and Pr are the Reynolds number and Prandtl number of air in the experiment, respectively, λ is the thermal conductivity of air in the experiment, d is the combustion chamber diameter, ρ is the density of air in the experiment, v is the gas flow rate in the experiment, μ is the dynamic viscosity of air in the experiment, α is the thermal diffusion coefficient, c is the specific heat capacity of air in the experiment, and $(Pr_f/Pr_w)^{0.25}$ is the physical property correction factor with the value of 1.00 in this study. By substituting various coefficients into the calculation, the convective heat transfer coefficient h in the experiment was 70.4. Then, the heat release from battery flame Q could be calculated as Equation (15).

$$Q = qAt = Ah \sum_{i=1}^5 \int_{t_{sv}}^{t_e} (T_{f,i} - T_a) dt \quad (15)$$

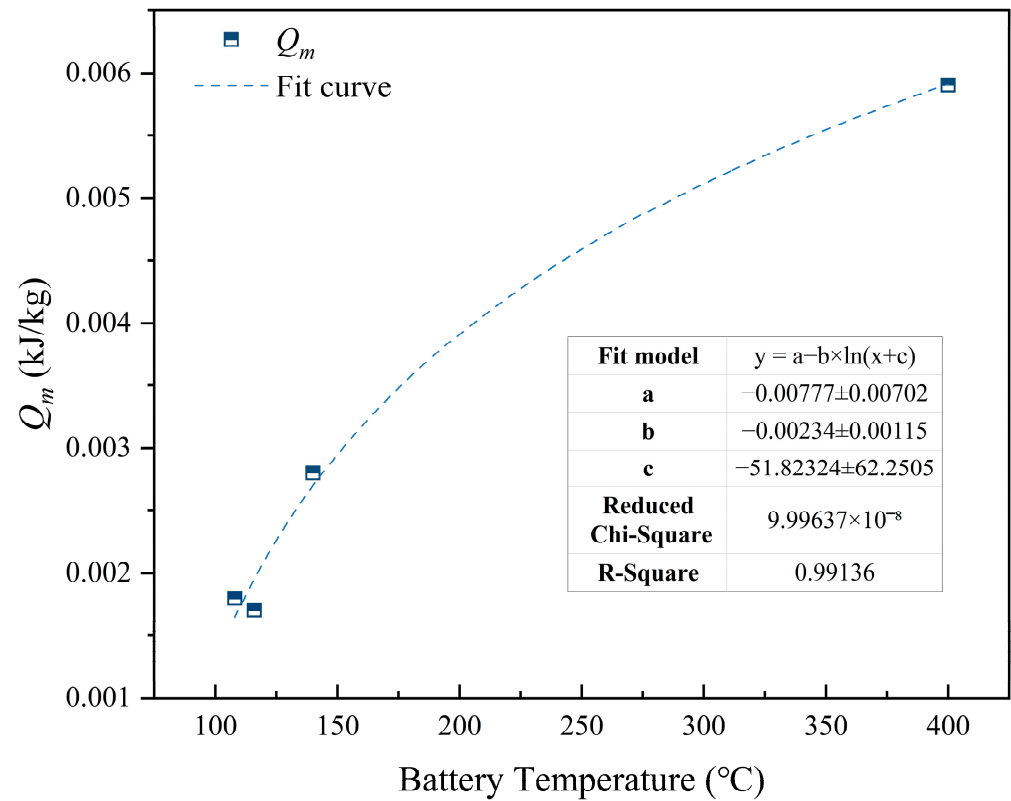
where A is the flame surface area assuming the flame shaping a cylinder, t_e and t_{sv} are the time of SV opening and TR ending, respectively. According to experimental videos, four time points of flame stabilizing after SV opening, TR triggering, flame peaking and TR ending were chosen to measure flame diameter and height. These were assumed to exhibit a linear variation between each two time points. The results for each case were 321.5 kJ in Case 1, 44.9 kJ in Case 2, 97.0 kJ in Case 3, 216.0 kJ in Case 4 and 284.4 kJ in Case 5. Using the time of SV opening, TR triggering and TR ending in Case 1 as the calculation reference, the differences in heat release between Case 1 and Cases 2 to 5 ΔQ were 11.6, 14.9, 54.4 and 37.1 kJ, respectively. Assuming the constant WM mass flow q_m , the specific cooling capacity of WM Q_m could be calculated by Equation (16). The results of each case are shown in Table 2.

$$Q_m = \frac{\Delta Q}{m_{WM}} = \frac{\Delta Q}{q_m \tau_{WM}} \quad (16)$$

where m_{WM} is the WM consumption for flame extinguishing and τ_{WM} is the release duration for WM to extinguish the flame. In order to clearly demonstrate the relationship between WM cooling and TR stages, Figure 5 is obtained by Q_m and battery temperature when WM is released.

Table 2. The heat release difference and specific cooling capacity of WM in Cases 2 to 5.

No.	ΔQ (kJ)	Q_m (kJ/kg)
Case 2	11.6	1.8×10^{-3}
Case 3	14.9	1.7×10^{-3}
Case 4	54.4	2.8×10^{-3}
Case 5	37.1	5.9×10^{-3}

**Figure 5.** The scatter plot of Q_m and the battery temperature when WM is released.

As shown in Figure 5, the scatter plot could be well fitted as the logarithmic function in the figure, and the specific cooling capacity of WM Q_m was increased with the increase in battery temperature (or TR process). It was because when the battery temperature was high, the velocity of the jet flame became more violent and the flame became higher. And if WM was released under a high battery temperature, the upper part of the battery flame would be compressed and cooled to a lower flame temperature in this region. This would significantly decrease the heat release from the flame and exhibit a higher Q_m . According to the fitting curve, Q_m at each WM released temperature could be roughly estimated, and the cooling effect of WM on battery flame was better after TR triggering.

In the TR process, the battery's upper surface would be exposed to flame radiation continuously which would directly affect other batteries of the module in practical LIB applications. Thus, it is of great significance to consider the flame radiation to the battery. In this experiment, the heat radiation of flame to the battery could be simplified to the average of five temperature measurement points, and the heat radiation power of each measurement point on the surface of the battery $P_{E,i}$ could be calculated as Equation (17) [41].

$$P_{E,i} = A_{\text{LIB}} \epsilon \frac{\sigma T_{E,i}^4}{4\pi L_i^2} \quad (17)$$

where A_{LIB} is the area of the battery's upper surface, ε is the surface emissivity of the aluminum battery surface which takes the value 0.05 [43], σ is the Stefan–Boltzmann constant, $T_{F,i}$ is the flame temperature at i position and L_i is the distance between i temperature measurement point and battery's upper surface. By integrating and averaging the $P_{E,i}$ of five measurement points, the heat radiation of flame to the battery's upper surface Q_E could be calculated as Equation (18).

$$Q_E = \frac{1}{5} \sum_{i=1}^5 \int_{t_{SV}}^{t_e} P_{E,i} dt = \frac{1}{5} A_{LIB} \varepsilon \sigma \sum_{i=1}^5 \frac{1}{4\pi L_i^2} \int_{t_{SV}}^{t_e} T_{F,i}^4 dt \quad (18)$$

The total flame heat radiation to the battery's upper surface in Case 1 was 117.33 kJ, and that of Cases 2 to 5 when WM released were 1.77, 0.56, 18.7 and 0.69 kJ, respectively. Also using the time of SV opening, TR triggering and TR ending in Case 1 as the calculation reference, the differences in flame heat radiation to the battery's upper surface between Case 1 and Cases 2 to 5 ΔQ_E were 5.83, 4.27, 26.31 and 1.94 kJ, respectively. Dividing ΔQ_E by the relative value of the reference case, the proportion of heat radiation cooling η in Cases 2 to 5 could be obtained. The calculation results of Cases 2 to 5 are shown in Table 3.

Table 3. The flame heat radiation to the battery's upper surface, its difference and cooling proportion in Cases 2 to 5.

No.	ΔQ_E (kJ)	η
Case 2	5.83	76.7%
Case 3	4.27	88.4%
Case 4	26.31	58.5%
Case 5	1.94	73.8%

As with the flame temperature above, after TR triggering, the battery flame was not directly extinguished and the temperatures of the flame bottom were still high. However, in the combustion process, the flame bottom was the main part affecting the heat radiation on the battery, resulting in a poorer suppression capacity for heat radiation. Although WM in Case 4 exhibited the poorest suppression effect, its η still reached 58.5%, implying a great suppression effect. For the whole TR process, WM released 3 min after SV opening exhibited the greatest suppression effect of flame heat radiation with the value of 88.4% which was the same for Q_m with the value of 1.7×10^{-3} kJ/kg.

4. Conclusions

During the TR process, a LIB undergoes distinct stages, including external heating, SV opening, TR triggering, and TR ending. The flame behavior varies significantly at each stage. After the SV opens, the battery flame exhibits a jet state, and its velocity intensifies following TR triggering. Prior to TR triggering, WM can effectively extinguish the battery flame, but its efficacy diminishes once TR is triggered. This study examined the impact of WM on battery flames at different TR stages, and the key findings are summarized as follows:

The flame extinguishing duration for WM under different TR stages was different. WM could directly put out the flame within several seconds released when SV opened, 3 min after SV opening and when TR ended, and it took about 3 min for WM to put out the flame released when TR triggered. When WM is released before TR triggering, the flame temperature exhibits a gradient, with lower temperatures at the top and higher temperatures at the bottom. Notably, the temperature at a position 10 cm above the SV reaches significantly higher values. Conversely, when WM is released after TR triggering, the temperatures at 30 cm and 50 cm are both higher. This observation correlates with uneven combustion at the base of the TR flame and compression at its apex.

The heat release of battery flame Q could be calculated by the flame temperatures, and Q in Cases 1 to 5 were 321.5, 44.9, 97.0, 216.0 and 284.4 kJ, respectively. Using the

time of SV opening, TR triggering and TR ending in Case 1 as the calculation reference, the differences in heat release between Case 1 and Cases 2 to 5 ΔQ were 11.6, 14.9, 54.4 and 37.1 kJ, respectively, and the specific cooling capacity of WM Q_m in Cases 2 to 5 were 1.8×10^{-3} , 1.7×10^{-3} , 2.8×10^{-3} and 5.9×10^{-3} kJ/kg, respectively. The results for Q_m could be well fitted as the logarithmic function, according to which, Q_m at each WM released temperature could be roughly estimated. Moreover, the heat radiation of flame to the battery Q_E could be calculated, and the case of WM released 3 min after SV opening exhibited the greatest proportion of heat radiation cooling η with the value of 88.4% which was the same for Q_m with the value of 1.7×10^{-3} kJ/kg.

This is expected to provide a novel focus for TR suppression in the LIB and make contributions to prevent further expansion of disasters from the perspective of TR flames.

Author Contributions: Conceptualization, B.M. and J.L.; methodology, B.M.; software, J.L.; validation, J.L.; formal analysis, B.M.; investigation, Q.W.; resources, B.M. and Q.W.; data curation, G.Z.; writing—original draft preparation, B.M.; writing—review and editing, C.G.; visualization, G.A.; supervision, J.O.; project administration, B.M. and Q.W.; funding acquisition, B.M. and Q.W. All authors have read and agreed to the published version of the manuscript.

Funding: This work was supported by the National Natural Science Foundation of China (NSFC) (52278359), Natural Science Foundation of Jiangsu Province (No. BK20221130) and General Program of National Natural Science Foundation of China (51974305).

Data Availability Statement: Dataset available on request from the authors.

Acknowledgments: The authors are thankful to all those who have contributed to the article and the funding support.

Conflicts of Interest: Author Bin Miao was employed by the company Zaozhuang Mining Group Co., Ltd and Guanzhang Zhu was employed by the company Beijing Tianma Intelligent Control Technology Co., Ltd. The remaining authors declare that the research was conducted in the absence of any commercial or financial relationships that could be construed as a potential conflict of interest.

Nomenclature

A	Flame surface area, m^2
A_{LIB}	Area of battery upper surface, m^2
c	Specific heat capacity of air, $J/(kg \cdot K)$
d	Combustion chamber diameter, m
h	Convective heat transfer coefficient, $W/(m^2 \cdot K)$
L_i	Distance between i temperature measurement point and battery's upper surface, m
m_{WM}	WM consumption for flame extinguishing, kg
Nu	Nusselt number
$P_{E,i}$	Heat radiation power of each measurement points on the surface of the battery, W
Pr	Prandtl number
$(Pr_f/Pr_w)^{0.25}$	Physical property correction factor
Q	Heat release of battery flame, J
Q_E	Heat radiation of flame to the battery, J
Q_m	Specific cooling capacity of WM, kJ/kg
ΔQ	Difference in heat release, J
ΔQ_E	Differences in flame heat radiation to battery's upper surface, J
q	Heat flux density of battery flame, W/m^2
q_m	WM mass flow, kg/s
Re	Reynolds number
T_a	Ambient temperature, $^{\circ}C$
$T_{E,i}$	Flame temperature at i position, K
$T_{f,i}$	Flame temperature at i position, $^{\circ}C$

t_e	Time of SV opening, s
t_{SV}	Time of TR ending, s
v	Gas flow rate, m/s
Abbreviations	
LIB	Lithium-ion Battery
LFP	Lithium Iron Phosphate
NCA	Nickel Cobalt Aluminum Ternary Lithium
NCM	Nickel Cobalt Manganese Ternary Lithium
SEI	Solid Electrolyte Interface
SOC	State of Charge
SOH	State of Health
SV	Safety Valve
TR	Thermal Runaway
WM	Water Mist
Greek	
λ	Thermal conductivity of air, W/(m·K)
ε	Surface emissivity of the aluminum battery surface
α	Thermal diffusion coefficient, m ² /s
η	Proportion of heat radiation cooling
μ	Dynamic viscosity of air, m ² /s
ρ	Density of air, kg/m ³
σ	Stefan–Boltzmann constant
τ_{WM}	Release duration for WM to extinguish the flame, s

References

- Hu, X.Y.; Liu, T.; Zhu, G.Q.; Cui, S.Q.; Huang, J.H.; Dong, X.T.; Guo, X.Y. Study on temperature heterogeneity and flame confrontation of LiFePO₄ battery thermal runaway inhibition by water mist. *Appl. Therm. Eng.* **2024**, *244*, 122675. [\[CrossRef\]](#)
- Li, Q.; Yu, J.S.; Liu, G.Z.; Ma, X.G.; Si, W.; Hu, X.Y.; Zhu, G.Q.; Liu, T. Study on the Effectiveness of Water Mist on Suppressing Thermal Runaway in LiFePO₄ Batteries. *Crystals* **2023**, *13*, 1346. [\[CrossRef\]](#)
- Liu, J.L.; Duan, Q.L.; Qi, K.X.; Liu, Y.J.; Sun, J.H.; Wang, Z.R.; Wang, Q.S. Capacity fading mechanisms and state of health prediction of commercial lithium-ion battery in total lifespan. *J. Energy Storage* **2022**, *46*, 103910. [\[CrossRef\]](#)
- Liu, T.; Huang, J.H.; Hu, X.Y.; Cui, S.Q.; Zhu, G.Q. Study on the variation of normalized heat and gas release of overcharge-induced thermal runaway in confined space. *Appl. Therm. Eng.* **2024**, *243*, 122636. [\[CrossRef\]](#)
- Zheng, Y.S.; Che, Y.H.; Hu, X.S.; Sui, X.; Stroe, D.I.; Teodorescu, R. Thermal state monitoring of lithium-ion batteries: Progress, challenges, and opportunities. *Prog. Energy Combust. Sci.* **2024**, *100*, 101120. [\[CrossRef\]](#)
- Al-Zareer, M.; Dincer, I.; Rosen, M.A. Comparative assessment of new liquid-to-vapor type battery cooling systems. *Energy* **2019**, *188*, 116010. [\[CrossRef\]](#)
- Feng, X.N.; He, X.M.; Ouyang, M.G.; Wang, L.; Lu, L.G.; Ren, D.S.; Santhanagopalan, S. A Coupled Electrochemical-Thermal Failure Model for Predicting the Thermal Runaway Behavior of Lithium-Ion Batteries. *J. Electrochem. Soc.* **2018**, *165*, A3748–A3765. [\[CrossRef\]](#)
- Wang, G.Q.; Kong, D.P.; Ping, P.; Wen, J.; He, X.Q.; Zhao, H.L.; He, X.; Peng, R.Q.; Zhang, Y.; Dai, X.Y. Revealing particle venting of lithium-ion batteries during thermal runaway: A multi-scale model toward multiphase process. *Etransportation* **2023**, *16*, 100237. [\[CrossRef\]](#)
- Cao, Y.F.; Wang, K.; Wang, Z.R.; Wang, J.L.; Yang, Y.; Xu, X.Y. Utilization of liquid nitrogen as efficient inhibitor upon thermal runaway of 18650 lithium ion battery in open space. *Renew. Energy* **2023**, *206*, 1097–1105. [\[CrossRef\]](#)
- Zhu, X.Q.; Wang, H.; Wang, X.; Gao, Y.F.; Allu, S.; Cakmak, E.; Wang, Z.P. Internal short circuit and failure mechanisms of lithium-ion pouch cells under mechanical indentation abuse conditions: An experimental study. *J. Power Sources* **2020**, *455*, 100237. [\[CrossRef\]](#)
- Gao, T.F.; Wang, Z.R.; Chen, S.C.; Guo, L.S. Hazardous characteristics of charge and discharge of lithium-ion batteries under adiabatic environment and hot environment. *Int. J. Heat Mass Transf.* **2019**, *141*, 419–431. [\[CrossRef\]](#)
- Mao, B.B.; Liu, C.Q.; Yang, K.; Li, S.; Liu, P.J.; Zhang, M.J.; Meng, X.D.; Gao, F.; Duan, Q.L.; Wang, Q.S.; et al. Thermal runaway and fire behaviors of a 300 Ah lithium ion battery with LiFePO₄ as cathode. *Renew. Sustain. Energy Rev.* **2021**, *139*, 110717. [\[CrossRef\]](#)
- Wang, Z.; Ouyang, D.X.; Chen, M.Y.; Wang, X.H.; Zhang, Z.; Wang, J. Fire behavior of lithium-ion battery with different states of charge induced by high incident heat fluxes. *J. Therm. Anal. Calorim.* **2019**, *136*, 2239–2247. [\[CrossRef\]](#)
- Han, Z.; Zhao, L.; Zhao, J.; Xu, G.; Liu, H.; Chen, M. An Experimental Study on the Thermal Runaway Propagation of Cycling Aged Lithium-Ion Battery Modules. *Fire* **2024**, *7*, 119. [\[CrossRef\]](#)
- Wang, B.X.; Zhou, Z.Z.; Li, L.; Peng, Y.; Cao, J.D.; Yang, L.Z.; Cao, B. Experimental study on thermal runaway and its propagation of large format prismatic lithium-ion batteries. *J. Energy Storage* **2022**, *55*, 105550. [\[CrossRef\]](#)

16. Feng, X.N.; Ouyang, M.G.; Liu, X.; Lu, L.G.; Xia, Y.; He, X.M. Thermal runaway mechanism of lithium ion battery for electric vehicles: A review. *Energy Storage Mater.* **2018**, *10*, 246–267. [[CrossRef](#)]
17. Wang, Q.S.; Ping, P.; Zhao, X.J.; Chu, G.Q.; Sun, J.H.; Chen, C.H. Thermal runaway caused fire and explosion of lithium ion battery. *J. Power Sources* **2012**, *208*, 210–224. [[CrossRef](#)]
18. Ghiji, M.; Novozhilov, V.; Moinuddin, K.; Joseph, P.; Burch, I.; Suendermann, B.; Gamble, G. A Review of Lithium-Ion Battery Fire Suppression. *Energies* **2020**, *13*, 5117. [[CrossRef](#)]
19. Golubkov, A.W.; Fuchs, D.; Wagner, J.; Wiltsche, H.; Stangl, C.; Fauler, G.; Voitic, G.; Thaler, A.; Hacker, V. Thermal-runaway experiments on consumer Li-ion batteries with metal-oxide and olivin-type cathodes. *Rsc Adv.* **2014**, *4*, 3633–3642. [[CrossRef](#)]
20. Zhong, G.B.; Mao, B.B.; Wang, C.; Jiang, L.; Xu, K.Q.; Sun, J.H.; Wang, Q.S. Thermal runaway and fire behavior investigation of lithium ion batteries using modified cone calorimeter. *J. Therm. Anal. Calorim.* **2019**, *135*, 2879–2889. [[CrossRef](#)]
21. Feng, L.; Jiang, L.H.; Liu, J.L.; Wang, Z.Y.; Wei, Z.S.; Wang, Q.S. Dynamic overcharge investigations of lithium ion batteries with different state of health. *J. Power Sources* **2021**, *507*, 230262. [[CrossRef](#)]
22. Liu, P.J.; Li, S.; Jin, K.Q.; Fu, W.D.; Wang, C.D.; Jia, Z.Z.; Jiang, L.H.; Wang, Q.S. Thermal Runaway and Fire Behaviors of Lithium Iron Phosphate Battery Induced by Overheating and Overcharging. *Fire Technol.* **2023**, *59*, 1051–1072. [[CrossRef](#)]
23. Wei, D.; Zhang, M.Q.; Zhu, L.P.; Chen, H.; Huang, W.S.; Yao, J.; Yuan, Z.C.; Xu, C.S.; Feng, X.N. Study on Thermal Runaway Behavior of Li-Ion Batteries Using Different Abuse Methods. *Batteries* **2022**, *8*, 201. [[CrossRef](#)]
24. Tao, C.F.; Zhu, Y.H.; Liu, Z.Q.; Li, R.; Chen, Z.Y.; Gong, L.L.; Liu, J.H. The experimental investigation of thermal runaway characteristics of lithium battery under different nitrogen concentrations. *J. Therm. Anal. Calorim.* **2023**, *148*, 12097–12107. [[CrossRef](#)]
25. Li, Y.W.; Jiang, L.H.; Huang, Z.H.; Jia, Z.Z.; Qin, P.; Wang, Q.S. Pressure Effect on the Thermal Runaway Behaviors of Lithium-Ion Battery in Confined Space. *Fire Technol.* **2023**, *59*, 1137–1155. [[CrossRef](#)]
26. Qiu, Y.S.; Jiang, F.M. A review on passive and active strategies of enhancing the safety of lithium-ion batteries. *Int. J. Heat Mass Transf.* **2022**, *184*, 122288. [[CrossRef](#)]
27. Yuan, S.; Chang, C.Y.; Yan, S.S.; Zhou, P.; Qian, X.M.; Yuan, M.Q.; Liu, K. A review of fire-extinguishing agent on suppressing lithium-ion batteries fire. *J. Energy Chem.* **2021**, *62*, 262–280. [[CrossRef](#)]
28. Zhang, L.; Li, Y.Q.; Duan, Q.L.; Chen, M.; Xu, J.J.; Zhao, C.P.; Sun, J.H.; Wang, Q.S. Experimental study on the synergistic effect of gas extinguishing agents and water mist on suppressing lithium-ion battery fires. *J. Energy Storage* **2020**, *32*, 101801. [[CrossRef](#)]
29. Sun, H.L.; Zhang, L.; Duan, Q.L.; Wang, S.Y.; Sun, S.J.; Sun, J.H.; Wang, Q.S. Experimental study on suppressing thermal runaway propagation of lithium-ion batteries in confined space by various fire extinguishing agents. *Process Saf. Environ. Prot.* **2022**, *167*, 299–307. [[CrossRef](#)]
30. Zhao, J.C.; Xue, F.; Fu, Y.Y.; Cheng, Y.; Yang, H.; Lu, S. A comparative study on the thermal runaway inhibition of 18650 lithium-ion batteries by different fire extinguishing agents. *Iscience* **2021**, *24*, 102854. [[CrossRef](#)]
31. Hill, D. *Considerations for ESS Fire Safety*; DNVGL: Byrum, Norway, 2017.
32. Tang, W.; Yuan, L.M.; Thomas, R.; Soles, J. Comparison of Fire Suppression Techniques on Lithium-Ion Battery Pack Fires. *Min. Metall. Explor.* **2023**, *40*, 1081–1087. [[CrossRef](#)]
33. Liu, T.; Tao, C.F.; Wang, X.S. Cooling control effect of water mist on thermal runaway propagation in lithium ion battery modules. *Appl. Energy* **2020**, *267*, 115087. [[CrossRef](#)]
34. Zhang, T.W.; Liu, H.; Song, J.W.; Wang, B.; Wang, Y.; Shuai, X.C.; Guo, Z.D. Synergistic inhibition effect on lithium-ion batteries during thermal runaway by N₂-twin-fluid liquid mist. *Case Stud. Therm. Eng.* **2022**, *37*, 102269. [[CrossRef](#)]
35. Li, L.X.; Chen, Z.; Lu, Y.; Zang, P.J.; Zhan, W.; Cheng, Y.H. Study on the suppression of thermal runaway of lithium-ion battery by water mist with different additives. *Energy Sources Part A-Recovery Util. Environ. Eff.* **2023**, *45*, 11349–11362. [[CrossRef](#)]
36. Zhang, L.; Duan, Q.L.; Xu, J.J.; Meng, X.D.; Sun, J.H.; Wang, Q.S. Experimental investigation on suppression of thermal runaway propagation of lithium-ion battery by intermittent spray. *J. Energy Storage* **2023**, *58*, 106434. [[CrossRef](#)]
37. Mei, J.; Shi, G.Q.; Liu, H.; Wang, Z.; Chen, M.Y. Experimental study on the effect of passive retardation method for thermal runaway mitigation of lithium-ion battery. *Appl. Therm. Eng.* **2023**, *230*, 120861. [[CrossRef](#)]
38. Lönnermark, A. TOXFIRE-Fire Characteristics and Smoke Gas Analysis in under-Ventilated Large-Scale Combustion Experiments. Tests in the ISO 9705 Room. 1996. Available online: <https://www.diva-portal.org/smash/get/diva2:962010/FULLTEXT01.pdf> (accessed on 6 June 2024).
39. Diaz, F.; Wang, Y.; Weyhe, R.; Friedrich, B. Gas generation measurement and evaluation during mechanical processing and thermal treatment of spent Li-ion batteries. *Waste Manag.* **2019**, *84*, 102–111. [[CrossRef](#)]
40. Lee, J.-H.; Hong, S.-H.; Lee, H.-S.; Park, M.-W. Study on Gas-Generating Property of Lithium-Ion Batteries. *Fire Sci. Eng.* **2021**, *35*, 1–8. [[CrossRef](#)]
41. Incropera, F.P.; DeWitt, D.P.; Bergman, T.L.; Lavine, A.S. *Fundamentals of Heat and Mass Transfer*; Wiley: New York, NY, USA, 1996; Volume 6.

42. Han, R.; Tang, M.; Wang, D.; Zhang, S. Numerical analysis of the convective heat transfer coefficient effect on lithium battery thermal diffusion when considering temperature effect. *Sci. Technol. Rev.* **2023**, *41*, 104–112.
43. Hu, Z. *Experimental Investigation of Steel and Aluminum Alloy Surface Emissivity Characteristics*; Henan Normal University: Xinxiang, China, 2010.

Disclaimer/Publisher's Note: The statements, opinions and data contained in all publications are solely those of the individual author(s) and contributor(s) and not of MDPI and/or the editor(s). MDPI and/or the editor(s) disclaim responsibility for any injury to people or property resulting from any ideas, methods, instructions or products referred to in the content.